Endocrinology, 2024, **165**, bqae064
https://doi.org/10.1210/endocr/bqae064
Advance access publication 5 June 2024
Research Article

Genetic Background Strongly Influences the Impact of Carrying the Thr92Ala-DIO2 Polymorphism in the Male Mouse

Guilherme Gabriel de Almeida,[1] Anaysa P. Bolin,[2] Alice Batistuzzo,[1] Tatiana L. Fonseca,[1] Miriam O. Ribeiro,[3] and Antonio C. Bianco[1]

[1]Section of Adult and Pediatric Endocrinology, Diabetes & Metabolism, University of Chicago Medical Center, Chicago, IL 60637, USA
[2]Department of Pharmacology, Biomedical Science Institute, University of São Paulo, São Paulo 05508, Brazil
[3]Human Developmental Sciences Graduate Program, Center for Biological and Health Sciences, Presbyterian Mackenzie University, São Paulo, SP 01302, Brazil

Correspondence: Antonio C. Bianco, MD, PhD, Section of Adult and Pediatric Endocrinology, Diabetes and Metabolism, University of Chicago, 5841 South Maryland Ave., Chicago, IL 60637, USA. Email: abianco@deiodinase.org.

Abstract

About half of the world population carries at least one allele of the Ala92-DIO2, which slows down the activity of the type 2 deiodinase (D2), the enzyme that activates T4 to T3. Carrying the Ala92-DIO2 allele has been associated with increased body mass index and insulin resistance, but this has not been reproduced in all populations. To test if the genetic background affects the impact of this polymorphism, here we studied the genetically distant C57Bl/6J (B6) and FVB/N (FVB) mice carrying the Ala92-Dio2 allele as compared to control mice carrying the Thr92-Dio2 allele. Whereas B6-Ala92-Dio2 and B6-Thr92-Dio2 mice—fed chow or high-fat diet—behaved metabolically similar in studies using indirect calorimetry, glucose- and insulin tolerance tests, and measuring white adipose tissue (WAT) weight and liver steatosis, major differences were observed between FVB-Ala92-Dio2 and FVB-Thr92-Dio2 mice: carrying the Ala92-Dio2 allele (on a chow diet) resulted in hypercholesterolemia, smaller WAT pads, hepatomegaly, steatosis, and transcriptome changes in the interscapular brown adipose tissue (iBAT) typical of ER stress and apoptosis. Acclimatization at thermoneutrality (30 °C) eliminated most of the metabolic phenotype, indicating that impaired adaptive (BAT) thermogenesis can be involved. In conclusion, the metabolic impact of carrying the Ala92-Dio2 allele depends greatly on the genetic background of the mouse, varying from no phenotype in B6 mice to a major phenotype in FVB mice. These results will help the planning of future clinical trials studying the Thr92Ala-DIO2 polymorphism and may explain why some clinical studies performed in different populations across the globe have obtained inconsistent results.

Key Words: deiodinases, thyroid hormone, lipids, steatosis

Abbreviations: ANOVA, analysis of variance; ApoA1, apolipoprotein A1; BAT, brown adipose tissue; CLAMS, comprehensive lab animal monitoring system; D2, type-2 deiodinase; EE, energy expenditure; ER, endoplasmic reticulum; ES, enrichment score; GTT, glucose tolerance test; HDL, high-density lipoprotein; HFD, high-fat diet; iBAT, interscapular brown adipose tissue; ITT, insulin tolerance test; LDL, low-density lipoprotein; PPARγ, peroxisome proliferator-activated receptor γ; RNA-seq, RNA sequencing; RQ, respiratory quotient; rT3, reverse T3; RT-qPCR, real-time quantitative polymerase chain reaction; SEM, standard error of the mean; SNP, single nucleotide polymorphism; T3, triiodothyronine; T4, thyroxine; UPR, unfolded protein response; VLDL, very low-density lipoprotein; WAT, white adipose tissue.

The Dio2 gene encodes the type-2 deiodinase (D2), an enzyme that activates thyroxine (T4) to triiodothyronine (T3), enhancing T3 signaling at its target tissue level. In many settings, Dio2 expression is in coordination with Dio3 expression, the gene that encodes the type 3 deiodinase (D3), which decreases T3 signaling by terminally inactivating T4 and T3. Through the selective expression of these enzymes, T3 signaling can be regulated in a tissue-specific fashion (1).

T3 plasma levels are relatively low in the mammalian embryo, hence the expression of these enzymes is critical to determine the timing of T3 effects during development (2). For example, Dio2 is expressed in the developing liver (murine and human) enhancing T3 signaling in hepatoblasts and the maturation into hepatocytes. It also defines how the liver handles fat in the adult mouse through epigenetic modifications of the hepatocyte chromatin (3-7). In the adult mouse, tissue-specific inactivation of Dio2 revealed multilevel control of adaptive thermogenesis and fatty acid oxidation by thyroid hormone (8). Whereas BAT D2 activity directly promotes adaptive thermogenesis (9, 10), brain D2 plays a dominant albeit indirect role in fatty acid oxidation via its sympathetic control of BAT activity (8).

Dio2 is a cAMP-dependent gene (11) and is also regulated by insulin and peroxisome proliferator-activated receptor γ (PPARγ) (12), the FOXO family of transcription factors (13), and dietary flavonols (14). Hence, it is logical that Dio2 plays an important metabolic role in tissues such as the hypothalamus, brown adipose tissue (BAT), skeletal muscle, and liver (15, 16).

The Dio2 gene exhibits a prevalent Thr92Ala-Dio2 (rs225014) polymorphism worldwide (about 50% of the population carries

Received: 21 March 2024. **Editorial Decision:** 30 May 2024. **Corrected and Typeset:** 17 June 2024

at least one Ala92 allele) that reduces the activity of the enzyme by 20% to 40% (17, 18) and has been associated with different conditions, including metabolic abnormalities such as increased body mass index and insulin resistance (19, 20), albeit not consistently across different populations (21). While many of these studies might have been underpowered to detect meaningful differences, it is known that associations between single nucleotide polymorphisms (SNPs) and specific traits are not reproduced across different populations (22). Such variability indicates that the phenotypic impact of SNPs can be modulated by the environment and by other genes and that interactions among different SNPs can also be heavily dependent on the genetic background in which they are studied (23-25).

To gain further insight into the role played by the Thr92Ala-Dio2 (rs225014) SNP, genetically modified C57Bl/6J (B6) mice were engineered to express either the Thr92-Dio2 or the Ala92-Dio2 alleles. However, preliminary studies failed to identify a meaningful metabolic phenotype (18). When compared to the B6-Thr92-Dio2 mouse, the B6-Ala92-Dio2 mouse failed to exhibit substantial differences in basic metabolic parameters (18). Inspired by the heterogeneity of the data obtained in humans, we hypothesized that the mouse genetic background could play a role (26). For example, the B6 mouse is widely used in metabolic studies because it is susceptible to diabetes and diet-induced obesity (27), insulin resistance, and dyslipidemia (28). In contrast, the genetically distant FVB/N (FVB) mouse (29) does not develop diet-induced obesity (28) and has persistent hyperinsulinemia with hyperglycemia when fed a high-fat diet (HFD) (30).

To test whether the metabolic impact of the Thr92Ala-Dio2 polymorphism is affected by the genetic background, here we studied the Thr92Ala-Dio2 polymorphism in B6 and FVB mice carrying the polymorphism. We now report that the FVB-Ala92-Dio2 mouse has reduced adiposity, hypercholesterolemia, and an enlarged liver with steatosis, a phenotype that is triggered by impaired BAT adaptive thermogenesis.

Material and Methods

Animals

The experiments were approved by the Institutional Animal Care and Use Committee of the University of Chicago (ACUP #72577). Male B6 or FVB mice carrying the Thr92-Dio2 or the Ala92-Dio2 alleles were used throughout the experiments (18). FVB-Thr92Ala-Dio2 mice were obtained by backcrossing B6-Thr92Ala-Dio2 mice to the FVB background for 8 generations. All mice were male, approximately 2 to 3 months old, and weighed between 20 and 30 g. All received water and food ad libitum and were maintained in a 12-hour day:night cycle. As indicated, some mice were placed on a HFD (Envigo Teklad Custom Diet [TD.06414] Teklad) for 14 weeks. Glucose tolerance test (GTT) and insulin tolerance test (ITT) were performed after 11 weeks on HFD (31). Animals were fasted overnight and given intraperitoneal glucose administration (1.5 g/kg of body weight). For the ITT, mice were fasted for 6 hours and received intraperitoneal administration of insulin (0.5 IU/kg body weight). Subsequently, blood samples were obtained from the tail vein and used for measuring glucose (31).

In some experiments, animals were admitted to a comprehensive lab animal monitoring system Oxymax® (CLAMS) to evaluate oxygen consumption (VO2), energy expenditure (EE), respiratory quotient (RQ), and food intake (31). Those parameters were measured for up to 64 days at 22 °C, 35 days at thermoneutrality conditions, and 32 days during gradual exposure to cold. Acclimatization to thermoneutrality was achieved by housing the animals in the CLAMS at 30 °C for 35 days. Progressive exposure to cold was performed by keeping the animals first at 22 °C for 8 days in the CLAMS followed by 13 days at 30 °C and subsequent decrease of the temperature: 4 days at 18 °C, 4 days at 10 °C and 3 days at 4 °C.

While in the CLAMS, animals were kept in individual cages. Food was withdrawn at 6 PM on the first day of the fasting experiments while they remained with free access to water. After overnight fasting, animals were euthanized through carbon dioxide (CO_2) inhalation. After death confirmation by pinching the paw, blood was collected from the heart, and several organs were dissected and weighed (liver, subcutaneous white adipose tissue [WAT], retroperitoneal WAT, epididymal WAT, and interscapular BAT (iBAT) (32).

Plasma Thyrotropin, T4, T3 and rT3 Analyses

To assess plasma thyroid hormone levels, the blood was collected in tubes containing K_2EDTA and allowed to sit overnight at 4 °C. Plasma was separated after blood was centrifuged for 15 minutes, 2000*g* at 4 °C, stored at −80 °C and processed for thyrotropin (thyroid-stimulating hormone; TSH) analysis using a MILLIPLEX rat TH panel kit (Millipore Corp.) and read on a BioPlex (Bio-Rad). Plasma levels of T4, T3, and reverse T3 (rT3) were assayed using radioimmunoassay (33).

Biochemical Analyses

Plasma cholesterol levels were measured using a commercial kit (Cholesterol/ Cholesteryl Ester Assay Kit; Abcam). Briefly, 5 µL of plasma was diluted 50 × in assay buffer in a 96-well plate. The reaction mix (2 µL esterase, 2 µL enzyme, 2 µL probe, and 44 µL of buffer) was added, followed by incubating at 37 °C for 1 hour. Samples were read at OD570 nm in a spectrophotometer Cytation 5 (BioTek). For the liver samples, we extracted 10 mg of the liver in 200 µL of chloroform:isopropanol:NP-40 (7:11:0.1) solution, centrifuged for 10 minutes at 15 000*g*, collected the supernatant, and air-dried. The pellet was dissolved in 200 µL of assay buffer and processed as above. High-density lipoprotein (HDL) and low-density lipoprotein (LDL)/very low-density lipoprotein (VLDL) cholesterol plasma levels were measured after 50 × dilution in assay buffer using a fluorometric assay (Cholesterol Assay Kit—HDL and LDL/VLDL; Abcam) read at 570 nm. Plasma triglyceride levels were measured using the Triglyceride Assay Kit (Abcam). Briefly, 10 µL of plasma was diluted 5 × in assay buffer in a 96-well plate and treated with 2 µL of lipase for 20 minutes. This was followed by the addition of 2 µL enzyme, 2 µL probe, and 46 µL of buffer per well. After incubation at 37 °C for 1 hour, samples were read at 570 nm. For liver samples, a homogenate was prepared with 20 mg of liver in 5% NP-40/ddH2O solution using a Dounce homogenizer. Samples were then slowly heated to 100 °C in a water bath and allowed to cool to room temperature; this step was repeated until the homogenate became cloudy. Plasma concentrations of apolipoprotein A1 (ApoA1) were measured using the Mouse ApoA1 ELISA Kit (Abcam Cat# ab238260, RRID:AB_3099642). After plasma samples were diluted 1:225 000 with assay buffer in a 96-well plate, they were read at 450 nm. For all the liver assays, the results were normalized by liver weight.

Table 1. Primers used for RT-qPCR gene expression analysis

Gene	Forward	Reverse
Abc-a1	CTTTCCTACTCTGTACCCGAGG	CGGGGCATTCCATTGATAAGG
Acc	GCCTCTTCCTGACAAACGAG	TGACTGCCGAAACATCTCTG
App	TCCGAGAGGTGTGCTCTGAA	CCACATCCGCCGTAAAAGAATG
Atf3	GAGGATTTTGCTAACCTGACACC	TTGACGGTAACTGACTCCAGC
Crym	GGGAGTCATGCCTGCCTAC	AGCCATTGCTGGGATCAAAGA
Cyp2a22	GGGGACCGCTTCAACTACG	GTCCAGGGTACTGTGGTTGTG
Dnajc10	GGAGCTGTCAACTGTGGTGAT	CCGATCTCCATTGTACTTCACTG
Edem1	GGGGCATGTTCGTCTTCGG	CGGCAGTAGATGGGGTTGAG
Fasn	GGAGGTGGTGATAGCCGGTAT	TGGGTAATCCATAGAGCCCAG
Fcgr2b	AGGGCCTCCATCTGGACTG	GTGGTTCTGGTAATCATGCTCTG
Fst	TGCTGCTACTCTGCCAGTTC	GTGCTGCAACACTCTTCCTTG
Gdpd3	CTCTCCTGTACTTTGTTCTGCC	CCAGGCGGATAGGGAAGAC
Gpam	ACAGTTGGCACAATAGACGTTT	CCTTCCATTTCAGTGTTGCAGA
Hsd17b6	GGAGCGTGTTGGAGACAGAG	GAGGTTCACTTGAAAGATAGGCA
Hspa5	ACTTGGGGACCACCTATTCCT	ATCGCCAATCAGACGCTCC
Hyou1	TGCGCTTCCAGATCAGTCC	GGAGTAGTTCAGAACCATGCC
Lcat	GTAACCACACACGGCCTGTC	TCTTACGGTAGCACATCCAGTT
Manf	TCTGGGACGATTTTACCAGGA	TCTTGCTTCACGGCAAAACTTTA
Ncor1	CTGCTCCGCATCAAGTGATAA	CCAGGAGTTCCCTGTGAGATA
Ncor2	GACGTGTCTCAGCAGTCGG	GCGTGTGGGGAAGTCTTGA
Osbpl5	TTCTGGGCTGCGAAAATGAG	GTCAGATCCATTGCATAGCCTG
Pgc1a	TATGGAGTGACATAGAGTGTGCT	CCACTTCAATCCACCCAGAAAG
Pgc1b	TCCTGTAAAAGCCCGGAGTAT	GCTCTGGTAGGGGCAGTGA
Ppara	AGAGCCCCATCTGTCCTCTC	ACTGGTAGTCTGCAAAACCAAA
Pparg	TCGCTGATGCACTGCCTATG	GAGAGGTCCACAGAGCTGATT
Ptpn1	GGAACTGGGCGGCTATTTACC	CAAAAGGGCTGACATCTCGGT
Rnf185	ATGGCAAGTAAAGGGCCTTCG	CACGGCCAACAGAAGAGGT
Scd1	TTCTTGCGATACACTCTGGTGC	CGGGATTGAATGTTCTTGTCGT
Selenbp2	AAGGGCTGGATGTTGCCAGAAATG	TGCAGCCAGTTGCTGAAGTAAAGG
Serinc3	GTCCCGTGCCTCTGTAGTG	CAAGACACAATAGTGCCAAGGAA
Socs3	ATGGTCACCCACAGCAAGTTT	TCCAGTAGAATCCGCTCTCCT
Spot14	ATGCAAGTGCTAACGAAACGC	CCTGCCATTCCTCCCTTGG
Syvn1	CGTGTGGACTTTATGGAACGC	CGGGTCAGGATGCTGTGATAAG
Tmem18	ATGGAGACAGACTGGACAGAG	TGCAGCCACTTCGTTGATGTA
Ube2g2	TGGCCGAGTATAAGCAATTAACC	GGCTCAAGGGGTAGTCAAGT
Ubqln2	GCCGAGCCCAAAATCATCAAA	ATCTTTCCGGCGAAAATCAGC
Yod1	GCCAAATCGCCGCTATCAC	ATGTCCCGGTCGCTGAGAT
Zdhhc23	GGCTGCCTGTTTGTGTGATTG	CCGTGATTCTTTCGCAAGTCTC
Zfp125	AAAGCCTTTCCAACACCCAG	TGTTCGAGTTGACTGCAGTTTT

Real-Time Quantitative Polymerase Chain Reaction

For real-time quantitative polymerase chain reaction (RT-qPCR) analysis, liver RNA was extracted with the RNeasy® Lipid Tissue Mini Kit (QIAGEN) as described previously (7). Briefly, 10 mg of liver was homogenized with Tissue-Tearor model 985370—Biospec Products, Inc. in Trizol (QIAzol Lysis Reagent—79306) and filtered with a spin column at 8000*g*. RNA quality was verified at 260 and 280 nm (Nanodrop Spectrophotometer/Fluorometer DS-11; DeNovix). cDNA was synthesized using Transcriptor First Strand cDNA Synthesis Kit (Roche) with 10 minutes cycles at 25 °C, 60 minutes at 50 °C, and 5 minutes at 85 °C, and it was quantified with the Nanodrop. RT-qPCR was performed using the 2kit (PowerUp™ SYBR™ Green Master Mix; Applied Biosystems) using cyclophilin B (Cyclo B) as the housekeeper gene (Table 1). Standard curves consisting of 5 points of serially diluted mixed experimental and control group cDNA were included. The coefficient of correlation was consistently > 0.98, with an amplification efficiency of 80% to 110%.

Next-Generation Sequencing

Extraction of iBAT RNA was performed using RNeasy (Lipid Tissue; QIAGEN). Libraries for next-generation RNA

sequencing (RNA-seq) were prepared with the (micro-array genotyping; Illumina) at the University of Chicago Core Facility and sequenced on the Illumina NovaSEQ-X with Oligo-dT mRNA directional Ribo-Zero depletion PE100 set reading for 30 to 60 M clusters/sample and ~50 to 60 M paired end reads/sample. All samples were treated with a kit (RNase-Free DNase; QIAGEN). RNA-Seq data were processed using the Partek Flow software. Data was alignment using the STAR 2.7.8 index tool and assembled using as reference the library *Mus musculus* mm10 whole genome. Gene counts were compiled using the GENCODE—M24 tool in counts per million. Analysis of variance (ANOVA) of FVB-Ala92-Dio2 vs FVB-Thr92-Dio2 samples was used to calculate the differential expression.

Liver Histology

Tissue preparation was done with fresh liver trimmed to a suitable size for embedding with O.C.T. compound (Tissue-Tek) and snap-frozen in dry ice. The embedded tissue was then stored at −80 °C until sectioning at the Human Tissue Resource Center at the University of Chicago. The staining was done with hematoxylin-eosin or with Oil Red O (Propylene Glycol Stain Kit; Newcomer supply). Briefly, tissue samples were fixed in 10% formalin for 1 minute, then immersed in propylene glycol 100% for 5 minutes. The samples were then incubated in the Oil Red O solution for 1 hour at room temperature under gentle agitation. After staining, the excess dye was removed with 85% propylene glycol, followed by distilled water, and counterstained with hematoxylin for 2 to 3 minutes. Finally, the slide was mounted with aqueous mounting media. The slides were scanned in Olympus VS200 Slideview Research Slide Scanner and analyzed in QuPath software (34) where the image contrast was adjusted to highlight the Oil Red O and then, fat droplets were detected with the pixel detect tool set with blue filter, sigma 3, and threshold 171.

Statistical Analysis

Values are expressed as mean ± standard error of the mean (SEM) (figures) or as mean ± SD (tables). Data were analyzed using GraphPad Prism software by one-tail Student *t* tests. Differences were considered statistically significant at $P < .05$.

Results

B6 mice carrying the Ala92-Dio2 polymorphism exhibit similar energy expenditure (EE), food intake, body weight, white and brown fat pads, and liver weight as compared to control B6-Thr92-Dio2 mice while on a chow diet (18). We attempted to bring out a metabolic phenotype by challenging the B6-Thr92-Dio2 and B6-Ala92-Dio2 mice with HFD for 14 weeks. Mice of both genotypes (Supplementary Fig. S1A) (35) gained ~24 g (control mice kept on a chow diet gained ~7 g/mouse) (Supplementary Fig. S1B) (35). Indirect calorimetry studies revealed no genotype-specific differences in VO2, EE, or RQ (Supplementary Fig. S2A-S2C) (35), and the contribution of fat oxidation to EE (Supplementary Fig. S2D) (35). Fasting glucose levels were also similar in mice of both genotypes (Supplementary Fig. S3A) (35). Feeding on the HFD led to a mild but similar degree of glucose intolerance (the area under the curve was slightly larger in the B6-Ala92-Dio2 mice; Supplementary Fig. S3B and S3C) (35) and insulin insensitivity (Supplementary Fig. S3D and S3E) (35).

The epididymal WAT depot was not affected by HFD in the B6-Thr92-Dio2 mice but it did increase by 60% in the B6-Ala92-Dio2 mice (Supplementary Fig. S4A) (35). In both mice, the subcutaneous and retroperitoneal WAT depots doubled in size (Supplementary Fig. S4A) (35) and the adipose index (the total of all WAT depots) increased by 60% to 100% (Supplementary Fig. S4B) (35). At the same time, the iBAT weight increased by about 2.3- to 3.0-fold (Supplementary Fig. S4C) (35) with HFD, independently of genotype. While on the chow diet, the liver of the B6-Ala92-Dio2 mice weighed similar to the B6-Thr92-Dio2 mice (Supplementary Fig. S5A) (35) and exhibited similar macroscopic (Supplementary Fig. S5B) (35) and histological aspects (Supplementary Fig. S5C and S5D) (35), namely, organ color and the size of the cells and amounts of lipids in the cytoplasm, respectively. After HFD, the weight of the B6-Ala92-Dio2 liver increased by about 1.6-fold whereas in the B6-Thr92-Dio2 the liver increased by 2-fold (Supplementary Fig. S5A) (35). In both mice, the liver developed a similar fatty aspect after HFD (Supplementary Fig. S5B) (35) and marked steatosis (Supplementary Fig. S5E and S5F) (35).

The FVB-Ala92-DIO2 Mouse Exhibits a Metabolic Phenotype

To test the effects of the Ala92-Dio2 on a genetically distant mouse strain, we next studied FVB-Thr92Ala-Dio2 mice. In contrast to B6-Ala92-Dio2 mice (which exhibit normal levels of TSH, T4, and T3 (18), the FVB-Ala92-Dio2 mice displayed slightly higher TSH plasma levels (0.47 ± 0.08 vs 1.05 ± 0.18 ng/mL, $n = 8$), lower plasma T4 (3.0 ± 0.30 vs 1.8 ± 0.32 ug/dL, $n = 8$) and unaffected plasma T3 levels (99 ± 3.3 vs 114 ± 8.9 ng/dL; $n = 8$). Despite these modest changes in thyroid function tests, these mice have preserved systemic T3-signaling, as indicated by the superimposed curves of food intake (Fig. 1A), body weight gain (Fig. 1B), VO2 (Fig. 1C), EE (Fig. 1D), and RQ (Fig. 1E) of FVB-Thr92- and FVB-Ala92-Dio2 mice. The tibial length was only minimally increased (~3%) in FVB-Ala92-Dio2 mice (Table 2).

There were notable metabolic differences between the FVB-Thr92-Dio2 and FVB-Ala92-Dio2 mice: (i) *hypercholesterolemia*: the Ala92-Dio2 mice exhibited ~30% higher plasma cholesterol, ~40% higher in plasma HDL cholesterol, and ~85% higher ApoA1 plasma levels, whereas plasma triglycerides and VLDL + LDL cholesterol levels were not different (Table 3); (ii) *smaller fat pad depots*: the WAT depots were 35% to 45% smaller (and the iBAT ~17% smaller) than observed in the FVB-Thr92-Dio2 mice (Table 2); (iii) *hepatomegaly and steatosis*: the liver of the FVB-Ala92-Dio2 mouse was ~15% heavier (g/mm tibial length) (Table 2) and contained ~3-fold more lipids as documented through histochemistry (Fig. 1F-1H) and direct measurement of triglycerides and cholesterol contents, which were 2.4-fold and ~25% higher in FVB-Ala92-Dio2 liver, respectively (Fig. 1I and 1J); (iv) *altered hepatic gene expression*: the mRNA levels for Ppar-α, Pgc1α, Pgc1β, and Zfp125 were 30%, 65%, 30%, and 27% higher, respectively, and those for Pparγ were 37% lower in the FVB-Ala92-Dio2 liver (Fig. 1K and 1L); the expression of other metabolically relevant genes (Abc-a1, Acc, Fasn, Gpam, Lcat, Ncor1, Ncor2, Scd1, Spot14, and Tmem18) was not different (Fig. 1K and 1L).

These differences in the FVB-Ala92-Dio2 mouse suggest that they exhibit an accelerated lipolysis which results in

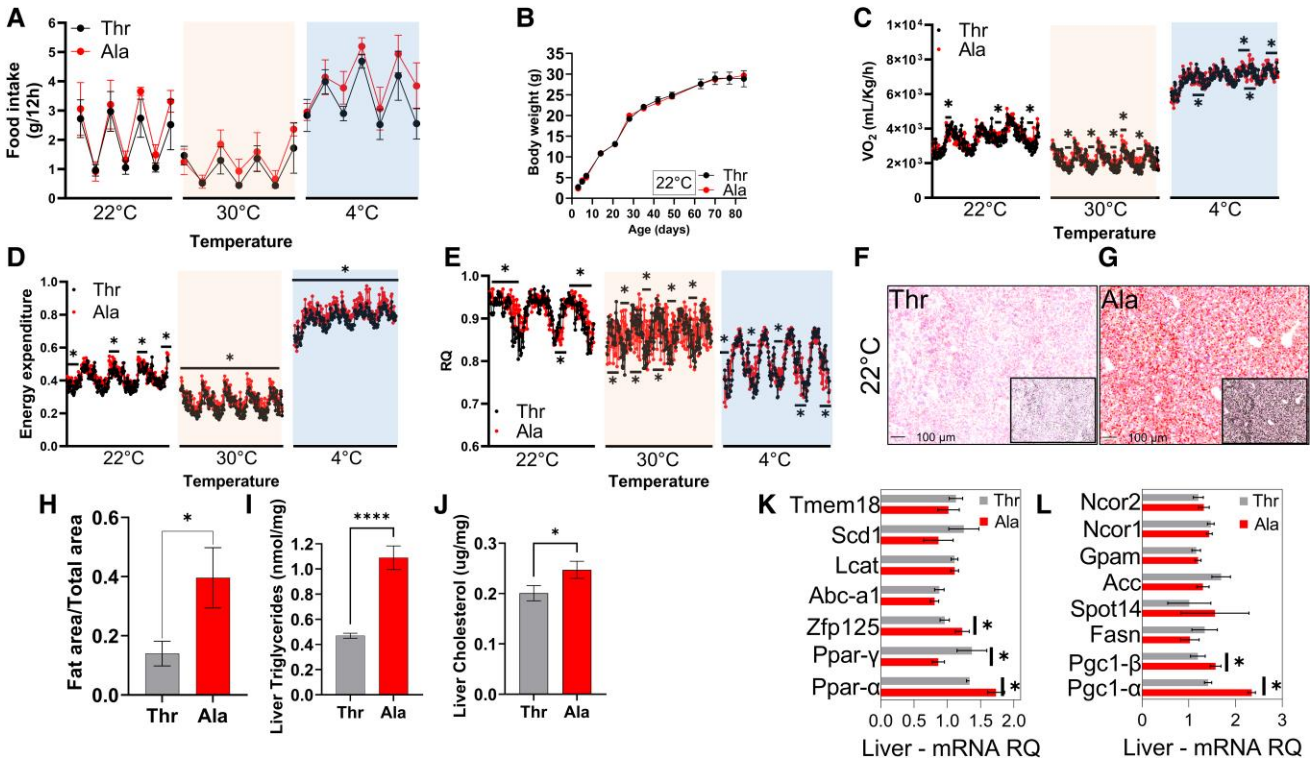

Figure 1. Studies of FVB-Thr92-Dio2 (Thr) and FVB-Ala92-Dio2 (Ala) mice acclimatized to 30 °C (n = 3 per group), 22 °C (n = 6 per group), or 4 °C (n = 5 per group). (A) Food intake; each point is the mean for the 12 hours (light) and 12 hours (dark). (B) Evolution of body weight of mice kept at 22 °C. (C-E) Indirect calorimetry of mice acclimated to 30 °C, 22 °C, and 4 °C; (C) VO2, oxygen consumption, (D) energy expenditure, (E) respiratory quotient (RQ). (F-H) Liver sections of mice acclimatized to 22 °C stained with Oil Red O for visualization and quantification of lipids; QuPath generated scale bars, 100 µm; magnification is ×40; Insets from the images are magnified 7 times to highlight the lipid-staining morphology. (I) Liver triglycerides levels (nmol/mg) in the 22 °C group. (J) Liver cholesterol levels in the 22 °C group. (K-L) mRNA levels of the indicated genes in the liver as measured by RT-qPCR. In all cases, values are the mean ± SEM. $P \leq .05$, $P^{****} \leq .0001$.

Table 2. Liver, iBAT, and WAT depots weight, and tibia length in FVB-Thr92-Dio2 and FVB-Ala92-Dio2 mice acclimatized at different temperatures

Temp.	Organ	*Thr*	*Ala*	*P* value
22 °C	Liver	62.1 ± 6.8	71.5 ± 5.8	.041[a]
	iBAT	7.03 ± 1.1	5.84 ± 1.1	.021[a]
	Subcutaneous fat	26.7 ± 7.1	17.3 ± 4.7	.036[a]
	Epididymal fat	69.2 ± 16.1	31.4 ± 9.6	.002[a]
	Retroperitoneal fat	15.5 ± 4.4	8.4 ± 3.3	.017[a]
	Tibia	18.1 ± 0.41	18.7 ± 0.23	.006[a]
30 °C	Liver	65.5 ± 4.1	62.3 ± 8.1	.647
	iBAT	9.4 ± 0.29	7.54 ± 0.27	.0007[a]
	Subcutaneous fat	25.4 ± 3.9	22.6 ± 2.6	.436
	Epididymal fat	45.7 ± 7.6	47.8 ± 15.8	.877
	Retroperitoneal fat	11.6 ± 2.3	15.5 ± 5.2	.388
	Tibia	17.5 ± 0.31	18.0 ± 0.12	.078
4 °C	Liver	63.4 ± 5.2	72.2 ± 6.4	.044[a]
	iBAT	9.4 ± 0.8	9 ± 1.0	.285
	Subcutaneous fat	10.9 ± 2.5	9.9 ± 3.7	.660
	Epididymal fat	16.8 ± 6.5	15.8 ± 6.4	.810
	Retroperitoneal fat	2.8 ± 1.4	4.2 ± 2.3	.290
	Tibia	18.1 ± 0.38	18.1 ± 0.14	.988

Values are expressed as mean ± SD and indicate the ratio of organ weight/tibia length (mg/mm). Group n = 5.
[a]$P < .05$.

excessive fat uptake and deposition in the liver, inducing the expression of genes involved in fatty acid oxidation and inhibiting lipogenesis.

Acclimatization to Thermoneutrality or Progressive Exposure to Cold

D2 is expressed in BAT (9, 10) and its targeted inactivation impairs BAT function, hence triggering a secondary increase in sympathetic activity and lipolysis (36). Given that Ala92-Dio2 is 20% to 40% catalytically less active (18), it is conceivable that at least part of the FVB-Ala92-Dio2 mouse phenotype is due to impaired BAT function and a compensatory increase in sympathetic activity. Therefore, we tested whether acclimatization to thermoneutrality (30 °C): which minimizes sympathetic activity—or progressive cold exposure (18→10→4 °C), which maximizes sympathetic activity—would modify the FVB-Ala92-Dio2 mouse phenotype.

Thermoneutrality

Maintaining the FVB-Ala92-Dio2 mice at 30 °C for 35 days led to the expected ~40% reduction in VO2 and EE, which during limited periods (either during the light or dark cycles) remained slightly faster in the FVB-Ala92-Dio2 mice (Fig. 2A and 2B). Thermoneutrality did not affect the RQ, but it did result in significant differences between the FVB-Thr92-Dio2 and the FVB-Ala92-Dio2 mice, which were, in general, small and fluctuating in both directions (Fig. 2C). Food intake decreased to about half at thermoneutrality but no differences between genotypes were observed (Fig. 2D), including in the body weight (Fig. 2A) and the tibial length (Table 2).

Table 3. Plasma levels of cholesterol, HDL, LDL + VLDL, triglycerides, and apolipoprotein A1 of FVB-Thr92-Dio2 and FVB-Ala92-Dio2 mice acclimatized at different temperatures

Temp	Organ	*Thr*	*Ala*	*P* value
22 °C	Total cholesterol	1.3 ± 0.15	1.7 ± 0.47	.005[a]
	HDL	0.71 ± 0.16	1.0 ± 0.07	.004[a]
	LDL + VLDL	0.10 ± 0.04	0.08 ± 0.03	.396
	ApoA1	35.1 ± 23.1	64.8 ± 11.3	.019[a]
	Triglycerides	0.15 ± 0.06	0.14 ± 0.14	.451
30 °C	Total cholesterol	2.5 ± 0.2	2.9 ± 0.70	.500
	HDL	0.44 ± 0.06	0.52 ± 0.05	.114
	LDL + VLDL	0.21 ± 0.01	0.21 ± 0.001	.229
	ApoA1	11.9 ± 2.1	10.1 ± 1.4	.131
	Triglycerides	0.72 ± 0.25	0.56 ± 0.06	.173
4 °C	Total cholesterol	1.0 ± 0.39	0.63 ± 0.34	.128
	HDL	0.12 ± 0.02	0.15 ± 0.06	.178
	LDL + VLDL	0.96 ± 0.13	0.56 ± 0.30	.027[a]
	ApoA1	6.4 ± 1.7	6.6 ± 3.5	.458
	Triglycerides	0.25 ± 0.11	0.26 ± 0.19	.423
22 °C 38 hours fasting	Total cholesterol	0.11 ± 0.05	0.13 ± 0.02	.321
	HDL	0.01 ± 0.005	0.01 ± 0.005	.477
	LDL + VLDL	0.02 ± 0.009	0.03 ± 0.008	.055
	ApoA1	2.2 ± 0.65	2.4 ± 1.6	.428
	Triglycerides	0.08 ± 0.01	0.08 ± 0.01	.493

Values are expressed as mean ± SD. Total cholesterol (µg/µL), plasma high-density lipoprotein (HDL) (µg/µL), plasma low-density lipoprotein (LDL) and very low-density lipoprotein (VLDL) (µg/µL), apolipoprotein A1 (mg/dL), and triglycerides (nmol/µL). Group n = 5.
[a]$P < .05$.

Acclimatization to thermoneutrality eliminated most of the FVB-Ala92-Dio2 metabolic phenotype. Plasma cholesterol and triglycerides increased, HDL and ApoA1 levels decreased, but no longer were there differences between the two genotypes (Table 3). In the FVB-Ala92-Dio2 mice, the weight of the fat pads increased (Table 2) and the liver decreased, both reaching the level detected in the FVB-Thr92-Dio2 mice (Table 2). In addition, the lipid excess previously observed in the FVB-Ala92-Dio2 liver (Fig. 2F-2J) and the differences in liver Pparα, Pgc1β, and Zfp125 mRNA levels were dissipated (Fig. 2K). Nonetheless, the iBAT remained ∼20% lighter (Table 2), and the liver mRNA levels for Pgc1α were ∼40% higher in the FVB-Ala92-Dio2 mice, whereas the Ppar-γ mRNA levels remained ∼50% lower in these animals (Fig. 2K).

Cold exposure

Exposure to progressively lower temperatures during 11 days (4 days at 18 °C → 4 days at 10 °C → 3 days at 4 °C) dramatically (∼2-fold) accelerated VO2, and EE while lowering the RQ by ∼20% in mice of both genotypes (Fig. 3A-3C), with a ∼5% greater acceleration in the FVB-Ala92-Dio2 mice (Fig. 2A and 2B). Although differences in the RQ were observed between genotypes, these were, in general, small and fluctuating in both directions (Fig. 3C). The food intake about doubled with the cold but with no differences between groups

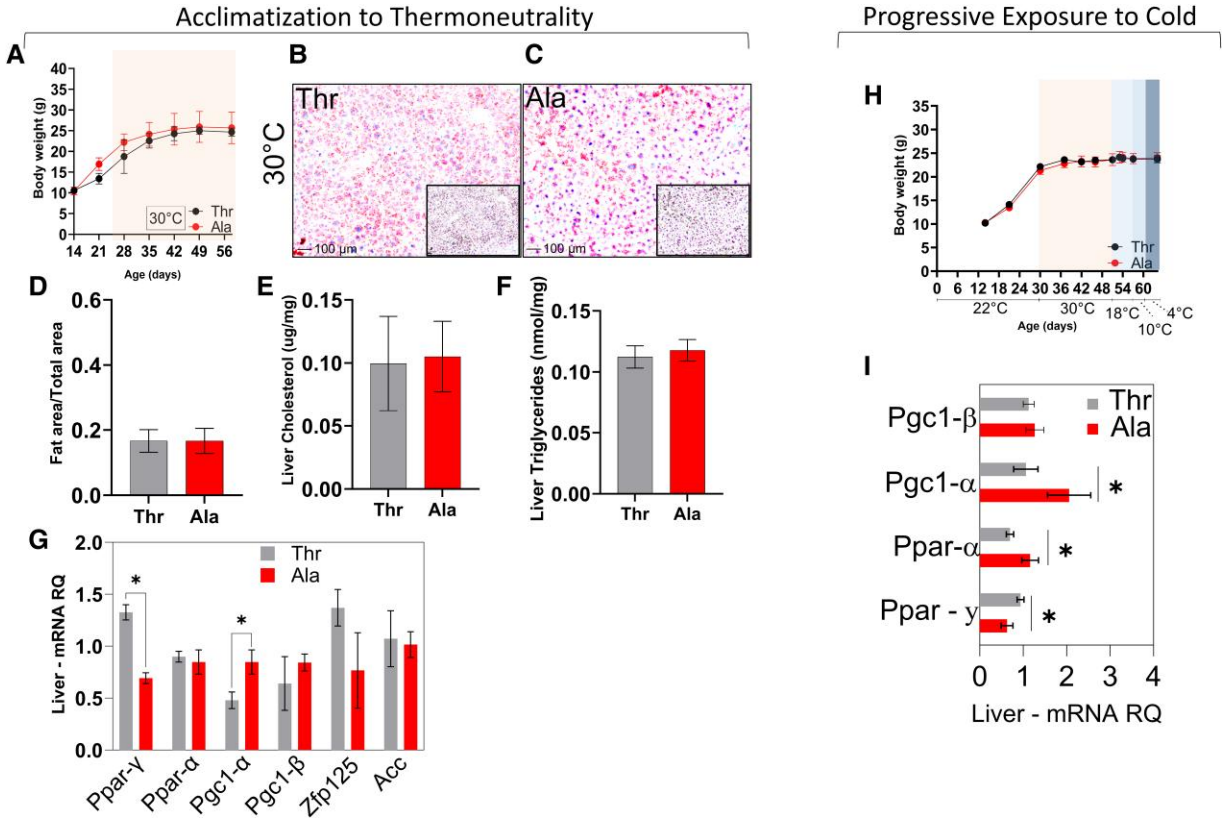

Figure 2. Studies of FVB-Thr92-Dio2 (Thr) and FVB-Ala92-Dio2 (Ala) mice acclimatized to 30 °C (n = 3 per group) and kept at progressive exposure to cold (n = 5 per group). (A) Evolution of body weight of mice acclimatized to 30 °C. (B-D) Liver sections of mice acclimatized to 30 °C stained with Oil Red O for visualization and quantification of lipids; QuPath generated scale bars, 100 µm; magnification is ×40; Insets from the images are magnified 7 times to highlight the lipid-staining morphology. (E) Liver cholesterol levels (ug/mg) in the 30 °C group. (F) Liver triglycerides levels (nmol/mg) in the 30 °C group. (G) mRNA levels of the indicated genes in the liver of mice acclimatized to 30 °C as measured by RT-qPCR. (H) Evolution of body weight of mice kept at progressive exposure to cold. (I) mRNA levels of the indicated genes in the liver of mice kept at progressive exposure to cold as measured by RT-qPCR. In all cases, values are mean ± SEM. *$P \leq .05$.

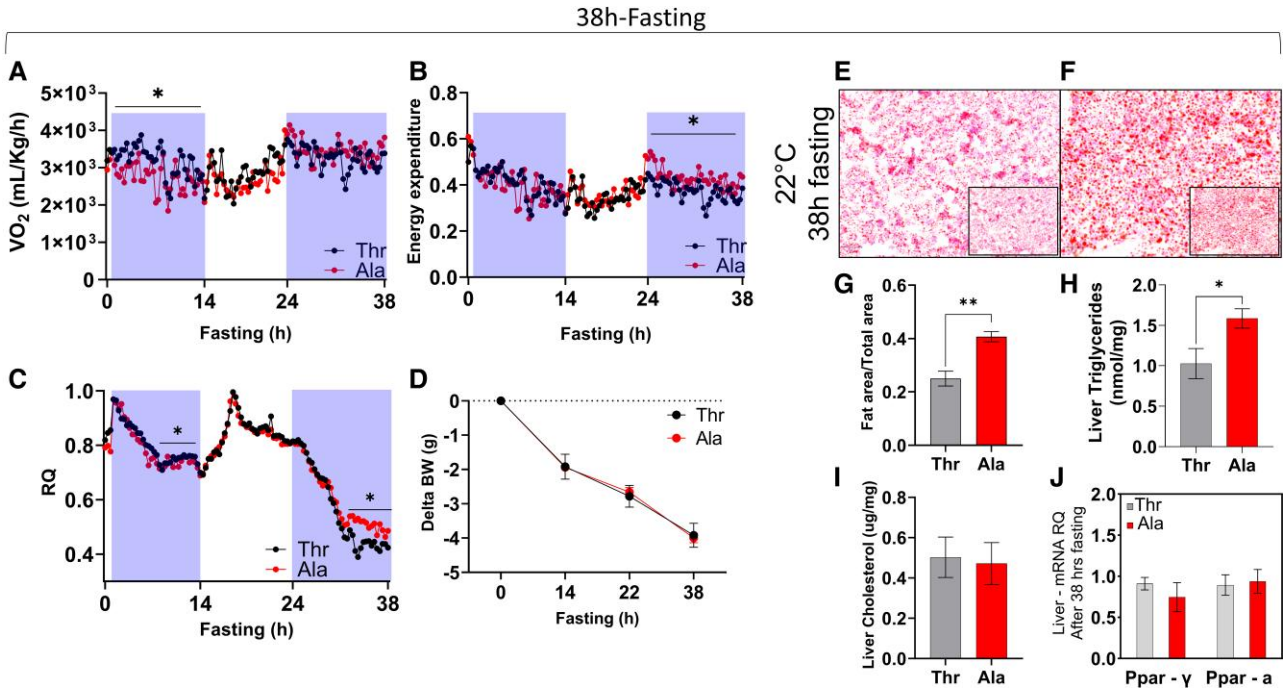

Figure 3. Studies of FVB-Thr92-Dio2 (Thr) and FVB-Ala92-Dio2 (Ala) mice acclimatized to 22 °C and undergoing 38 hours fasting (n = 5 per group). (A-C) Indirect calorimetry; (A) VO2, oxygen consumption, (B) energy expenditure, (C) respiratory quotient (RQ). (D) Body mass index loss throughout 38 hours of fasting. (E-G) Liver sections of mice acclimatized to 22 °C and undergoing 38 hours stained with Oil Red O for visualization and quantification of lipids; QuPath generated scale bars, 100 μm; magnification is ×40; Insets from the images are magnified seven times to highlight the lipid-staining morphology. (H) Liver triglycerides levels (nmol/mg). (I) Liver cholesterol levels (ug/mg). (J) mRNA levels of the indicated genes in the liver as measured by RT-qPCR. In all cases, values are mean ± SEM. $^{*}P \leq .05$.

(Fig. 3D). Likewise, the body weight (Fig. 2E), and the tibial length remained unaffected by exposure to cold (Table 2). In general, cold exposure markedly reduced HDL cholesterol and ApoA1 levels while increasing LDL + VLDL cholesterol and triglyceride levels, eliminating the differences between genotypes (Table 3). However, the plasma VLDL + LDL cholesterol levels were ~50% lower in FVB-Ala92-Dio2 (Table 3).

Cold exposure led to the expected reduction in the weight of the WAT pads and an increase in the weight of the iBAT, eliminating the differences between genotypes detected at room temperature (Table 2). Notably, the FVB-Ala92-Dio2 liver continued to be ~15% heavier (Table 2) and to exhibit higher mRNA levels for Pparα ~30% and Pgc1α ~65% (Fig. 3F) and lower mRNA levels for Pparγ ~30% (Fig. 2F). No differences were observed between genotypes for the Pgc1β mRNA levels (Fig. 2F).

Fasting

Fasting is also known to activate lipolysis and accelerate the flow of fatty acids to the liver. Fasting for 38 hours (1 light cycle and 2 dark cycles) caused a ~33% reduction in VO2 and EE as compared to animals kept with food ad libitum (Fig. 3A and 3B). Notably, only during the first 14 hours of fasting did the FVB-Ala92-Dio2 exhibit a slightly slower VO2 (Fig. 3A), whereas on the last 14 hours of fasting, they exhibited a slightly faster EE (Fig. 3B). As expected, the RQ levels dropped markedly as fasting progressed, with no differences between the genotypes (Fig. 3C), except for the last 7 hours of fasting when the FVB-Ala92-Dio2 mice maintained a substantially higher RQ (Fig. 3C). At the same time, the loss in body weight was similar in both genotypes (Fig. 3D).

Table 4. Liver and WAT weights, and tibia length in FVB-Thr92-Dio2 and FVB-Ala92-Dio2 mice after a 38-hour fast

Temp	Organ	*Thr*	*Ala*	*P* value
22 °C	Liver	49.7 ± 5.17	61.3 ± 11.1	.034[a]
	WAT	19.7 ± 13.9	11.9 ± 5.2	.027[a]
	Tibia	18.5 ± 0.72	18.9 ± 0.67	.175

Values are expressed as mean ± SD and indicate the ratio of organ weight/tibia length (mg/mm). Group n = 5.
[a]$P < .05$.

Fasting was also associated with a marked decrease in plasma lipid levels, but no differences were observed between both genotypes (Table 3). Notably, even after 38 hours of fasting the WAT depot remained ~40% lighter in the FVB-Ala92-Dio2 mice whereas the liver was ~23% heavier (Table 4) and exhibited higher lipid content (Fig. 3E-3G) and triglyceride levels (Fig. 3H), but the cholesterol content was similar in both genotypes (Fig. 3I). No differences in liver mRNA for Ppar-α and Ppar-γ were observed between groups (Fig. 3J).

Next-Generation Sequencing

The metabolic phenotype exhibited by the FVB-Ala92-Dio2 mice was almost eliminated by acclimatization at thermoneutrality, suggesting that the BAT is a key organ underlying this phenotype. To gain deeper insight into the molecular mechanisms involved, we processed the iBAT of FVB-Ala92-Dio2 mice that had been acclimatized to thermoneutrality. This allowed us to identify pathways that were altered by the local expression of the Ala92-Dio2 and not by the compensatory

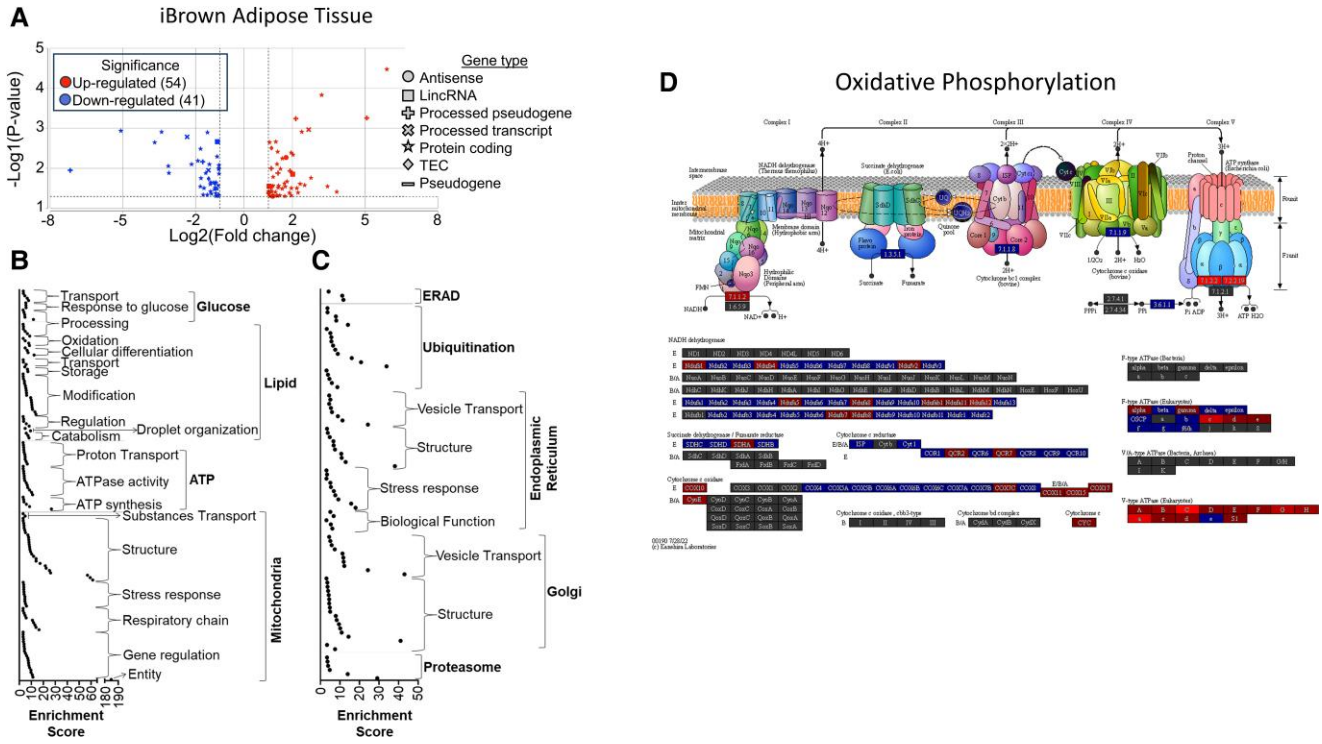

Figure 4. iBAT RNA-seq analysis of FVB-Ala92-Dio2 (Ala) vs FVB-Thr92-Dio2 (Thr) mice (n = 3 per group). (A) Volcano plot of the top 95 genes up- and downregulated, $P < .05$ and FDR < 0.25. (B-C) iBAT Gene Set Enrichment Analysis (GSEA). Gene sets organized by Gene Ontology (GO); (B) gene sets involved with mitochondrion, ATP, lipid, and glucose, (C) gene sets involved with proteasome, Golgi, endoplasmic reticulum, ubiquitination, and ERAD. (D) Oxidative phosphorylation pathway. Blue color (dots with a negative fold change) indicates downregulated genes and red (dots with a positive fold change) indicates overexpressed genes. Statistical analysis was performed using one-way ANOVA, $P < .05$ and FDR < 0.25. Abbreviation: iBAT, interscapular brown adipose tissue.

elevation in the sympathetic activity, which was eliminated by thermoneutrality.

The RNA-seq data was processed for ANOVA and filtered by $P < .05$ and fold > 2 and < −2, leading to 95 differentially expressed genes (54 upregulated and 41 downregulated) in the FVB-Ala92-Dio2 when compared to the FVB-Thr92-Dio2 iBAT (Fig. 4A; Supplementary Table S1) (35). Among the top 10 upregulated genes is Aqp11 (6.8-fold), shown to contribute to TGF-β1-induced endoplasmic reticulum (ER) stress in human visceral adipocytes (37), and among the top 10 downregulated genes are Gchfr (−34-fold), one of the genes that define browning (38) and Lgr6 (−8.7-fold), a receptor that mediates activation of BAT thermogenesis (39).

A comprehensive analysis of the RNA-seq data revealed 1900 gene sets enriched in the FVB-Ala92-Dio2 iBAT ($P < .05$ and FDR < 0.25), including 61 sets involved in glucose and lipid metabolism (enrichment score [ES] = 3.1-14) (Fig. 4B), 100 gene sets involved in ATP metabolism and mitochondria (ES = 3.1-185) (Fig. 4B), 29 gene sets involved ERAD, ubiquitination, and proteasomes (ES = 3.1-34), and 61 gene sets involved in ER and Golgi apparatus (ES = 3.1-43) (Supplementary Table S2) (35) (Fig. 4C). This indicates that expression of Ala92-Dio2 triggers ER stress and unfolded protein response (UPR), and affects major metabolic pathways involved in mitochondrial function.

An analysis of the gene pathways identified 96 pathways that were modified in the FVB-Ala92-Dio2 iBAT ($P < .05$; FDR < 0.18) (Supplementary Table S3) (35), including spliceosome (activation—ES = 26) (Supplementary Fig. S6) (35), the core machine that executes alternative splicing, which is a critical component of gene expression (some of the downstream splicing targets include mTOR, Pparγ, and Prdm16) (40). Autophagy (activation—ES = 26) (Supplementary Fig. S7) (35), participates in the intracellular remodeling events that occur during the transition from brown/beige to WAT (41), such as seen during acclimatization to thermoneutrality.

There is also a major activation of ER protein processing (activation—ES = 22) (Supplementary Fig. S8) (35), diseases linked to misfolded proteins (activation—Parkinson ES = 19, Alzheimer ES = 12.8, Amyotrophic Lateral Sclerosis ES = 12.5, Prion ES = 11.2, Huntington ES = 10) (Supplementary Fig. S9-S13) (35), ubiquitin-mediated proteolysis (activation—ES = 12) (Fig. 5A), and proteasome (activation—ES = 5.9) (Fig. 5B). All of these pathways are likely linked to the expression of Ala92-D2, a misfolded protein shown to cause ER stress in the brains of mice (18) and humans (42). One of the downstream targets of ER stress is apoptosis, which is also activated (ES = 7.4) (Supplementary Fig. S14) (35) in the FVB-Ala92-Dio2 iBAT.

Metabolic signaling is also affected in the iBAT of the FVB-Ala92-Dio2 mouse. Insulin signaling (activation—ES = 9.5) (Supplementary Fig. S15) (35), AMPK signaling (activation—9.2) (Supplementary Fig. S16), mTOR signaling (mixed—ES = 8.8) (Supplementary Fig. S17) (35), thyroid hormone signaling (inactivation—ES = 6.9) (Supplementary Fig. S18) (35), Notch signaling (activation—ES = 6.4) (Supplementary Fig. S19) (35), HIF-1 signaling (activation—ES = 5.7) (Supplementary Fig. S20) (35), glucagon signaling (mixed—ES = 3.5) (Supplementary Fig. S21) (35).

Along with these major changes in key BAT pathways, there is a downregulation of oxidative phosphorylation (ES = 19) (Fig. 4D), which explains the impaired adaptive BAT thermogenesis observed in the FVB-Ala92-Dio2 mouse.

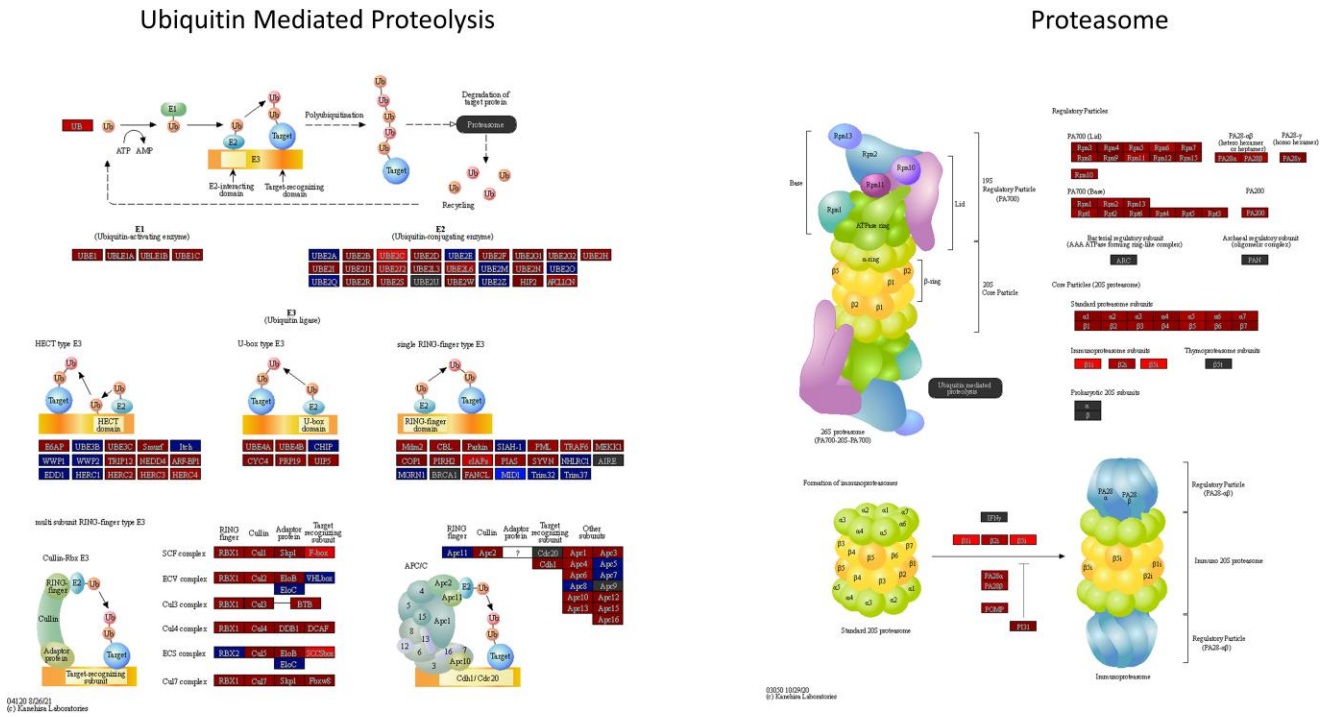

Figure 5. iBAT RNA-seq analysis of FVB-Ala92-Dio2 (Ala) vs FVB-Thr92-Dio2 (Thr) mice (n = 3 per group). (A) Ubiquitin-mediated proteolysis pathway. (B) Proteasome pathway. Blue color indicates downregulated genes and red indicates overexpressed genes. Statistical analysis was performed using one-way ANOVA, $P < .05$ and FDR < 0.25. Abbreviation: iBAT, interscapular brown adipose tissue.

Discussion

In the present investigation, we failed to trigger a meaningful metabolic phenotype in the B6-Ala92-Dio2 mouse even as they were challenged with HFD. Nonetheless, maintaining FVB-Ala92-Dio2 mice on a standard chow diet was sufficient to trigger a major metabolic phenotype. Only the FVB-Ala92-Dio2 mouse exhibits hepatomegaly, and liver steatosis accompanied by reduced adiposity and hypercholesterolemia (when compared to the FVB-Thr92-Dio2 mouse). Notably, most of the FVB-Ala92-Dio2 phenotype was eliminated after acclimatization to thermoneutrality (which reduces sympathetic activity), including restoration of the WAT depots to their normal size and elimination of hepatomegaly and liver steatosis.

These data suggest that the FVB-Ala92-Dio2 mouse has impaired adaptive thermogenesis, which triggers a compensatory increase in sympathetic activity even when at room temperature. While this adjustment in sympathetic activity sustains EE and thermal homeostasis, it also accelerates lipolysis. In addition, the FVB-Ala92-Dio2 liver seems unable to handle the increased influx of fatty acids, thus developing hepatomegaly and steatosis.

Room temperature (21 °C) can be a significant thermal stress for small rodents such as the mouse, as their thermal neutral temperature is closer to 28 °C. Hence, they must constantly maintain a degree of adaptive thermogenesis to preserve thermal homeostasis, that is, core temperature at 37 °C. In the case of the FVB-Ala92-Dio2 mouse, preserving thermal homeostasis requires a superactivation of the sympathetic activity, which promotes lipolysis and reduces adiposity. Based on other mouse models (inactivation of the UCP1 gene (43) or the Dio2 gene (36)), such an acceleration in sympathetic activity at room temperature is seen when BAT-mediated adaptive thermogenesis is impaired. This is a central point in the pathogenesis of the FVB-Ala92-Dio2 mouse phenotype.

Notably, carrying the Ala92-DIO2 allele in humans is unlikely to accelerate sympathetic activity or lipolysis. We lose much less heat to the environment than small rodents do, because of our smaller surface-to-volume ratio. In addition, clothing and other facilities help us to stay at or near thermoneutrality most of the time. Thus, carrying the Ala92-DIO2 SNP in certain populations has been associated with increased body mass index and insulin resistance (21).

The BAT is the main site of adaptive thermogenesis in small rodents. Dio2 is highly expressed in BAT and plays a key thermogenic role in enhancing T3 signaling (10, 44-46). The Ala92-D2 is 20% to 40% less catalytically active (17, 18); hence, it generates less T3 during BAT activation. Thus, it is logical to assume that BAT is the site of impaired adaptive thermogenesis in the FVB-Ala92-Dio2 mouse. In addition, Ala92-D2 is a misfolded protein that accumulates in the Golgi apparatus (42) and triggers ER stress in cells, the mouse (18), and the human brains (42). This is important because ER stress can potentially limit the BAT thermogenic capacity (47). To explore this further and cast a wide net over the BAT transcriptome, we performed an RNA-seq analysis of the FVB-Ala92-Dio2 iBAT of mice acclimated at thermoneutrality.

Our unbiased approach to studying gene expression in the FVB-Ala92-Dio2 iBAT revealed that the activation of ER stress and UPR is massive and agrees with our previous observations in the brain (18, 42, 48). Together with reduced catalytic activity (Ala92-D2), the ER stress and UPR triggered by the Ala92-D2 expression could explain the impaired thermogenic capacity of the FVB-Ala92-Dio2 BAT. The latter was documented through the 19-fold downregulation of the oxidative

phosphorylation gene pathway. The iBAT exhibited changes in other important pathways as well, such as spliceosome, autophagy, apoptosis, and several cell signaling pathways, all capable of reducing the ability for adaptive thermogenesis.

The inability of the FVB-Ala92-Dio2 liver to handle an increased influx of fatty acids caused by accelerated lipolysis at room temperature is the other central point in the pathogenesis of the mouse phenotype. This could explain the hepatomegaly, steatosis, and hypercholesterolemia. This is supported by the elimination of the phenotype when FVB-Ala92-Dio2 mice were acclimatized at thermoneutrality and by the presence of the phenotype when FVB-Ala92-Dio2 mice were progressively exposed to cold or fasting, both conditions known to trigger intense lipolysis. In both conditions, the FVB-Ala92-Dio2 mouse retained the hepatomegaly when compared to the FVB-Thr92-Dio2 mouse; and during fasting, their livers exhibited a much higher lipid content as well. These data support the concept that the FVB-Ala92-Dio2 liver cannot handle a lipid excess, which is in contrast to the B6-Ala92-Dio2 liver. When placed on HFD, the B6-Ala92-Dio2 mouse did not exhibit worse hepatomegaly or steatosis as compared to the B6-Thr92-Dio2 mouse.

The present findings suggest that the more severe phenotype observed in the FVB-Ala92-Dio2 mouse, particularly in BAT and liver, is associated with inherent characteristics of the FVB genetic background. In contrast, the B6-Ala92-Dio2 mouse maintains adaptive thermogenesis in BAT, even at room temperature, without signs of heightened sympathetic activity. This could be attributed to various factors such as the greater capacity of B6 iBAT to manage misfolded proteins, reduced sensitivity to ER stress, or other compensatory mechanisms. Additionally, the FVB liver appears to have an intrinsic predisposition to develop steatosis. Even under standard dietary conditions, the FVB liver exhibits elevated mRNA levels for Dgat-2 (1.7 times), Pparα (1.4 times), and Acox2 (1.2 times), while showing decreased mRNA levels for Apob (0.6 times) compared to B6 mice (28). When subjected to an HFD, FVB mice demonstrate increased insulin resistance and severe liver steatosis, indicating reduced efficiency in handling excess fat compared to B6 mice (28). Such an unfavorable metabolic setting might contribute to the liver steatosis of the FVB-Ala92-DIO2 mice at room temperature.

The present data are remarkable because they revealed the Thr92Ala-Dio2 (rs225014) polymorphism as a major metabolic disruptor, the impact of which depends greatly on the overall genetic context of the mouse. To the extent that these findings are translatable to humans, they would explain the inconsistent results obtained when assessing the metabolic impact of carrying the Thr92Ala-Dio2 (rs225014) polymorphism in different countries/populations (19-21).

In summary, the findings of this study suggest that harboring the Ala92-Dio2 allele may pose a significant risk for impaired adaptive thermogenesis, hypercholesterolemia, and liver steatosis, contingent upon genetic background. While the B6 mouse strain appears to mitigate this risk effectively, the FVB mouse strain does not. If applicable to humans, these results may elucidate the varying effects of the Thr92Ala-DIO2 polymorphism observed across different populations. It is plausible that the metabolic risks associated with the Thr92Ala-DIO2 polymorphism could also be influenced by other well-established factors contributing to metabolic imbalance, such as diet, alcohol consumption, and sedentary lifestyle, which may exacerbate its effects.

Acknowledgments

This work was supported by the National Institute of Diabetes and Digestive and Kidney Diseases (NIDDK –DK58538, DK65066, DK77148) (A.C.B.).

Funding

This work was supported by the National Institute of Diabetes and Digestive and Kidney Diseases NIDDK –DK58538, DK65066, DK77148 (A.C.B.); Fundação de Amparo à Pesquisa do Estado de São Paulo FAPESP 2016/10114-1 (A.P.B.); 2021/12746-3 (M.O.R.); Coordenação de Aperfeiçoamento de Pessoal de Nível Superior #2017/2023 88881.910035/2023-01 (M.O.R.)

Author Contributions

G.G.d.A.: performed experiments; analysis of the results, preparation of original writing draft, review & editing. A.P.B.: performed experiments with B6 mice; analysis of the results. A.B.: performed experiments; analysis of the results, review & editing. T.F.: performed experiments; analysis of the results. M.O.R.: conceptualization, review of manuscript. A.C.B.: conceptualization, funding acquisition, writing of original draft, review, and editing.

Disclosures

A.C.B. is a consultant for Abbvie, Allergan, Aligos, and Synthonics. The other authors have no relevant disclosures.

Data Availability

All data sets generated during and/or analyzed during the present study are included in the manuscript.

References

1. Bianco AC, Dumitrescu A, Gereben B, *et al*. Paradigms of dynamic control of thyroid hormone signaling. *Endocr Rev*. 2019;40(4):1000-1047.
2. Galton VA. The roles of the iodothyronine deiodinases in mammalian development. *Thyroid*. 2005;15(8):823-834.
3. Hidalgo-Alvarez J, Salas-Lucia F, Vera Cruz D, Fonseca TL, Bianco AC. Localized T3 production modifies the transcriptome and promotes the hepatocyte-like lineage in iPSC-derived hepatic organoids. *JCI Insight*. 2023;8(23):e173780.
4. Fonseca TL, Garcia T, Fernandes GW, Nair TM, Bianco AC. Neonatal thyroxine activation modifies epigenetic programming of the liver. *Nat Commun*. 2021;12(1):4446.
5. Fonseca TL, Fernandes GW, Bocco B, *et al*. Hepatic inactivation of the type 2 deiodinase confers resistance to alcoholic liver steatosis. *Alcohol Clin Exp Res*. 2019;43(7):1376-1383.
6. Fernandes GW, Bocco BM, Fonseca TL, *et al*. The FoxO1-inducible transcriptional repressor Zfp125 causes hepatic steatosis and hypercholesterolemia. *Cell Rep*. 2018;22(2):523-534.
7. Fonseca TL, Fernandes GW, McAninch EA, *et al*. Perinatal deiodinase 2 expression in hepatocytes defines epigenetic susceptibility to liver steatosis and obesity. *Proc Natl Acad Sci U S A*. 2015;112(45):14018-14023.
8. Fonseca TL, Werneck-De-Castro JP, Castillo M, *et al*. Tissue-specific inactivation of type 2 deiodinase reveals multilevel control of fatty acid oxidation by thyroid hormone in the mouse. *Diabetes*. 2014;63(5):1594-1604.

9. Hall JA, Ribich S, Christoffolete MA, *et al.* Absence of thyroid hormone activation during development underlies a permanent defect in adaptive thermogenesis. *Endocrinology*. 2010;151(9):4573-4582.
10. de Jesus LA, Carvalho SD, Ribeiro MO, *et al.* The type 2 iodothyronine deiodinase is essential for adaptive thermogenesis in brown adipose tissue. *J Clin Invest*. 2001;108(9):1379-1385.
11. Canettieri G, Celi FS, Baccheschi G, Salvatori L, Andreoli M, Centanni M. Isolation of human type 2 deiodinase gene promoter and characterization of a functional cyclic adenosine monophosphate response element. *Endocrinology*. 2000;141(5):1804-1813.
12. Grozovsky R, Ribich S, Rosene ML, *et al.* Type 2 deiodinase expression is induced by peroxisomal proliferator-activated receptor-gamma agonists in skeletal myocytes. *Endocrinology*. 2009;150(4):1976-1983.
13. Lartey LJ, Werneck-de-Castro JP IOS, Unterman TG, Bianco AC. Coupling between nutrient availability and thyroid hormone activation. *J Biol Chem*. 2015;290(51):30551-30561.
14. da-Silva WS, Harney JW, Kim BW, *et al.* The small polyphenolic molecule kaempferol increases cellular energy expenditure and thyroid hormone activation. *Diabetes*. 2007;56(3):767-776.
15. Russo SC, Salas-Lucia F, Bianco AC. Deiodinases and the metabolic code for thyroid hormone action. *Endocrinology*. 2021;162(8):bqab059.
16. Peeters R, Fekete C, Goncalves C, *et al.* Regional physiological adaptation of the central nervous system deiodinases to iodine deficiency. *Am J Physiol Endocrinol Metab*. 2001;281(1):E54-E61.
17. Castagna MG, Dentice M, Cantara S, *et al.* DIO2 thr92ala reduces deiodinase-2 activity and serum-T3 levels in thyroid-deficient patients. *J Clin Endocrinol Metab*. 2017;102(5):1623-1630.
18. Jo S, Fonseca TL, Bocco B, *et al.* Type 2 deiodinase polymorphism causes ER stress and hypothyroidism in the brain. *J Clin Invest*. 2019;129(1):230-245.
19. Mentuccia D, Proietti-Pannunzi L, Tanner K, *et al.* Association between a novel variant of the human type 2 deiodinase gene Thr92Ala and insulin resistance: evidence of interaction with the Trp64Arg variant of the beta-3-adrenergic receptor. *Diabetes*. 2002;51(3):880-883.
20. Maia AL, Dupuis J, Manning A, *et al.* The type 2 deiodinase (DIO2) A/G polymorphism is not associated with glycemic traits: the Framingham Heart Study. *Thyroid*. 2007;17(3):199-202.
21. Mentuccia D, Thomas MJ, Coppotelli G, *et al.* The Thr92Ala deiodinase type 2 (DIO2) variant is not associated with type 2 diabetes or indices of insulin resistance in the old order of Amish. *Thyroid*. 2005;15(11):1223-1227.
22. Penna GC, Salas-Lucia F, Ribeiro MO, Bianco AC. Gene polymorphisms and thyroid hormone signaling: implication for the treatment of hypothyroidism. *Endocrine*. 2023;84(2):309-319.
23. Mullis MN, Matsui T, Schell R, Foree R, Ehrenreich IM. The complex underpinnings of genetic background effects. *Nat Commun*. 2018;9(1):3548.
24. Chandler CH, Chari S, Kowalski A, *et al.* How well do you know your mutation? Complex effects of genetic background on expressivity, complementation, and ordering of allelic effects. *PLoS Genet*. 2017;13:e1007075.
25. Lachance J, Tishkoff SA. SNP ascertainment bias in population genetic analyses: why it is important, and how to correct it. *Bioessays*. 2013;35(9):780-786.
26. Haluzik M, Colombo C, Gavrilova O, *et al.* Genetic background (C57BL/6J versus FVB/N) strongly influences the severity of diabetes and insulin resistance in ob/ob mice. *Endocrinology*. 2004;145(7):3258-3264.
27. Fontaine DA, Davis DB. Attention to background strain is essential for metabolic research: C57BL/6 and the international knockout mouse consortium. *Diabetes*. 2016;65(1):25-33.
28. Nascimento-Sales M, Fredo-da-Costa I, Borges Mendes ACB, *et al.* Is the FVB/N mouse strain truly resistant to diet-induced obesity? *Physiol Rep*. 2017;5(9):e13271.
29. Beck JA, Lloyd S, Hafezparast M, *et al.* Genealogies of mouse inbred strains. *Nat Genet*. 2000;24(1):23-25.
30. Chua S Jr, Liu SM, Li Q, Yang L, Thassanapaff VT, Fisher P. Differential beta cell responses to hyperglycaemia and insulin resistance in two novel congenic strains of diabetes (FVB- Lepr (db)) and obese (DBA- Lep (ob)) mice. *Diabetologia*. 2002;45(7):976-990.
31. Castillo M, Hall JA, Correa-Medina M, *et al.* Disruption of thyroid hormone activation in type 2 deiodinase knockout mice causes obesity with glucose intolerance and liver steatosis only at thermoneutrality. *Diabetes*. 2011;60(4):1082-1089.
32. Cao Y, Gomes SA, Rangel EB, *et al.* S-nitrosoglutathione reductase-dependent PPARgamma denitrosylation participates in MSC-derived adipogenesis and osteogenesis. *J Clin Invest*. 2015;125(4):1679-1691.
33. Bianco AC, Anderson G, Forrest D, *et al.* American thyroid association guide to investigating thyroid hormone economy and action in rodent and cell models: report of the American Thyroid Association Task Force on Approaches and Strategies to investigate thyroid hormone economy and action. *Thyroid*. 2014;24(1):88-168.
34. Bankhead P, Loughrey MB, Fernández JA, *et al.* Qupath: open source software for digital pathology image analysis. *Sci Rep*. 2017;7(1):16878.
35. Gabriel de Almeida G, Bolin AP, Batistuzzo A, Fonseca TL, Ribeiro MO, Bianco AC. Genetic background (FVB/N versus C57BL/6J) strongly influences the impact of carrying the Thr92Ala-DIO2 polymorphism in the male mouse. *Zenodo*. 2024. Doi:10.5281/zenodo.11521673.
36. Christoffolete MA, Linardi CC, de Jesus L, *et al.* Mice with targeted disruption of the Dio2 gene have cold-induced overexpression of the uncoupling protein 1 gene but fail to increase brown adipose tissue lipogenesis and adaptive thermogenesis. *Diabetes*. 2004;53(3):577-584.
37. Frühbeck G, Balaguer I, Méndez-Giménez L, *et al.* Aquaporin-11 contributes to TGF-(1-induced endoplasmic reticulum stress in human visceral adipocytes: role in obesity-associated inflammation. *Cells*. 2020;9(6):1403.
38. Rosell M, Kaforou M, Frontini A, *et al.* Brown and white adipose tissues: intrinsic differences in gene expression and response to cold exposure in mice. *Am J Physiol Endocrinol Metab*. 2014;306(8):E945-E964.
39. Laiglesia LM, Escoté X, Sáinz N, *et al.* Maresin 1 activates brown adipose tissue and promotes browning of white adipose tissue in mice. *Mol Metab*. 2023;74:101749.
40. Naing YT, Sun L. The role of splicing factors in adipogenesis and thermogenesis. *Mol Cells*. 2023;46(5):268-277.
41. Cairó M, Villarroya J. The role of autophagy in brown and beige adipose tissue plasticity. *J Physiol Biochem*. 2020;76(2):213-226.
42. McAninch EA, Jo S, Preite NZ, *et al.* Prevalent polymorphism in thyroid hormone-activating enzyme leaves a genetic fingerprint that underlies associated clinical syndromes. *J Clin Endocrinol Metab*. 2015;100(3):920-933.
43. Feldmann HM, Golozoubova V, Cannon B, Nedergaard J. UCP1 ablation induces obesity and abolishes diet-induced thermogenesis in mice exempt from thermal stress by living at thermoneutrality. *Cell Metab*. 2009;9(2):203-209.
44. Bianco AC, Silva JE. Intracellular conversion of thyroxine to triiodothyronine is required for the optimal thermogenic function of brown adipose tissue. *J Clin Invest*. 1987;79(1):295-300.
45. Bianco AC, Silva JE. Optimal response of key enzymes and uncoupling protein to cold in BAT depends on local T3 generation. *Am J Physiol*. 1987;253(3 Pt 1):E255-E263.
46. Bianco AC, Silva JE. Nuclear 3,5,3(-triiiodothyronine (T3) in brown adipose tissue: receptor occupancy and sources of T3 as determined by in vivo techniques. *Endocrinology*. 1987;120(1):55-62.
47. Qiang G, Whang Kong H, Gil V, Liew CW. Transcription regulator TRIP-Br2 mediates ER stress-induced brown adipocytes dysfunction. *Sci Rep*. 2017;7(1):40215.
48. Lorena FB, Sato JM, Coviello BM, *et al.* Age worsens the cognitive phenotype in mice carrying the Thr92Ala-DIO2 polymorphism. *Metabolites*. 2022;12(7):629.